Available online at www.sciencedirect.com
ScienceDirect
Geochimica et Cosmochimica Acta 75 (2011) 1357–1373
Geochimica et Cosmochimica Acta
www.elsevier.com/locate/gca

Carbon, sulfur, and oxygen isotope evidence for a strong depth gradient and oceanic oxidation after the Ediacaran Hankalchough glaciation

Bing Shen [a,*], Shuhai Xiao [b], Huiming Bao [c], Alan J. Kaufman [d], Chuanming Zhou [e], Xunlai Yuan [e]

[a] Department of Earth Sciences, Rice University, Houston, TX 77005, USA
[b] Department of Geosciences, Virginia Polytechnic Institute and State University, Blacksburg, VA 24061, USA
[c] Department of Geology and Geophysics, Louisiana State University, Baton Rouge, LA 70803, USA
[d] Department of Geology, University of Maryland, College Park, MD 20742, USA
[e] State Key Laboratory of Paleobiology and Stratigraphy, Nanjing Institute of Geology and Paleontology, Chinese Academy of Sciences, Nanjing 210008, China

Received 19 January 2010; accepted in revised form 22 December 2010; available online 30 December 2010

Abstract

In order to understand spatial variations of stable isotope geochemistry in the Quruqtagh basin (northwestern China) in the aftermath of an Ediacaran glaciation, we analyzed carbonate carbon isotopes ($\delta^{13}C_{carb}$), carbonate oxygen isotopes ($\delta^{18}O_{carb}$), carbonate associated sulfate sulfur ($\delta^{34}S_{CAS}$) and oxygen isotopes ($\delta^{18}O_{CAS}$), and pyrite sulfur isotopes ($\delta^{34}S_{py}$) of a cap dolostone atop the Ediacaran Hankalchough glacial diamictite at four sections. The four studied sections (YKG, MK, H and ZBS) represent an onshore–offshore transect in the Quruqtagh basin. Our data show a strong paleobathymetry-dependent isotopic gradient. From the onshore to offshore sections, $\delta^{13}C_{carb}$ values decrease from −2‰ to −16‰ (VPDB), whereas $\delta^{18}O_{carb}$ values increase from −4‰ to −1‰ (VPDB). Both $\delta^{34}S_{CAS}$ and $\delta^{34}S_{py}$ show stratigraphic variations in the two onshore sections (MK and YKG), but are more stable in the two offshore sections (H and ZBS). $\delta^{18}O_{CAS}$ values of onshore samples are consistent with terrestrial oxidative weathering of pyrite. We propose that following the Hankalchough glaciation seawater in the Quruqtagh basin was characterized by a strong isotopic gradient. The isotopic data may be interpreted using a three-component mixing model that involves three reservoirs: deep-basin water, surface water, and terrestrial weathering input. In this model, the negative $\delta^{13}C_{carb}$ values in the offshore sections are related to the upwelling of deep-basin water (where anaerobic oxidation of dissolved organic carbon resulted in ^{13}C-depleted DIC), whereas sulfur isotope variations are strongly controlled by surface water sulfate and terrestrial weathering input derived from oxidative weathering of pyrite. The new data provide evidence for the oceanic oxidation following the Hankalchough glaciation.

1. INTRODUCTION

The Ediacaran Period experienced a transition from a Proterozoic-style anoxic/euxinic deep ocean that likely hosted a large reservoir of dissolved organic carbon (DOC) to a Phanerozoic-style oxic deep ocean dominated by dissolved inorganic carbon (DIC) (Canfield, 1998; Rothman et al., 2003; Canfield et al., 2008; Swanson-Hysell et al., 2010). Although there is evidence for an episodic oxidation and regional variation in the oxidation state of Ediacaran seawater (Fike et al., 2006; Canfield et al., 2007; Kaufman et al., 2007; McFadden et al., 2008; Scott et al., 2008; Shen et al., 2008; Ries et al., 2009), the causes and

* Corresponding author. Tel.: +1 281 733 6317.
E-mail addresses: bingshen66@gmail.com (B. Shen), xiao@vt.edu (S. Xiao).

0016-7037/$ - see front matter © 2010 Elsevier Ltd. All rights reserved.
doi:10.1016/j.gca.2010.12.015

processes responsible for the Ediacaran oxidation event are poorly understood.

Geological and geochemical evidence suggests that the Ediacaran oxidation event might have been temporally associated with glaciations (Fike et al., 2006; Canfield et al., 2007; Kaufman et al., 2007; Peltier et al., 2007). Unlike the globally-distributed Marinoan glacial diamictite of the Cryogenian Period (Hoffman et al., 1998; Hoffmann et al., 2004; Condon et al., 2005), glaciations in the Ediacaran Period were possibly regional and diachronous (Bowring et al., 2003; Xiao et al., 2004; Halverson et al., 2005; Corkeron, 2007). One of the Ediacaran glaciations—the Gaskiers glaciation in Newfoundland—is temporally associated with the rise of macroscopic life forms (the Ediacara biota) and deep ocean oxidation, implying a possible linkage between the Ediacaran glaciation, redox evolution, and biological evolution (Canfield et al., 2007); in Newfoundland, complex Ediacara fossils have been recorded in the >579 Ma Drook Formation that was deposited shortly after the ~582 Ma Gaskiers glaciation (Narbonne and Gehling, 2003; Hoffman and Li, 2009).

To further decipher Ediacaran redox history and to explore the possible linkage between Ediacaran glaciations and oceanic oxidation, we investigated the post-glacial Hankalchough cap dolostone atop the Ediacaran Hankalchough glacial diamictite in the Quruqtagh area of eastern Chinese Tianshan, northwestern China (Fig. 1). We focus on coupled multiple stable isotope measurements of cap dolostone at four sections representing an onshore–offshore transect of the Quruqtagh basin. Previously, $\delta^{13}C_{carb}$ and $\delta^{18}O_{carb}$ data from these successions were reported by Xiao et al. (2004). In this paper, we present sulfur and oxygen isotope data of carbonate associated sulfate (CAS) and sulfur isotope of disseminated pyrite that were extracted from the same samples analyzed by Xiao et al. (2004).

2. GEOLOGICAL SETTING

The Neoproterozoic Quruqtagh Group in the Quruqtagh area (Fig. 1) was deposited in a Neoproterozoic rift basin following the breakup of Rodinia at ~750 Ma (Xu et al., 2005). The Quruqtagh Group is dominated by siliciclastic deposits with volcanic interbeds. Diamictites occur in the Bayisi, Altungol, Tereeken, and Hankalchough formations (Gao and Zhu, 1984; Xiao et al., 2004). These diamictites have been interpreted as glacial deposits (Gao and Zhu, 1984), although convincing evidence for glaciation is noted only for the Tereeken and Hankalchough formations (Xiao et al., 2004; Xu et al., 2009). SHRIMP zircon U–Pb ages constrain the Tereeken diamictite between 726 ± 10

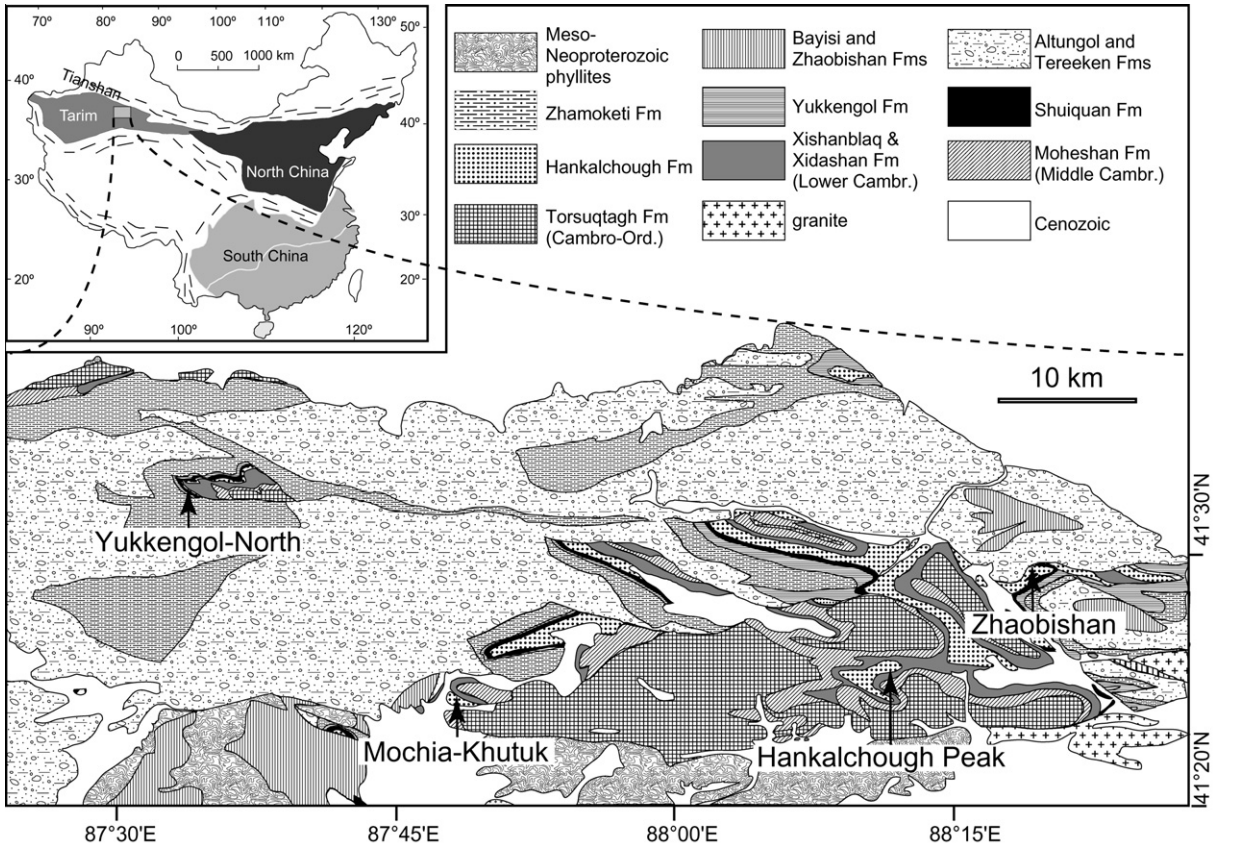

Fig. 1. Geological map (adopted from Xiao et al., 2004) showing location of the four studied sections of the Hankalchough cap dolostone in the Quruqtagh area, eastern Chinese Tianshan: Yukkengol-North section (YKG); Mochia–Khutuk section (MK); Hankalchough peak section (H); and Heishan–Zhaobishan section (ZBS). YKG-MK-H-ZBS represent an onshore–offshore transect. Inset shows the location of the Quruqtagh area (box) in the northeastern Tarim block.

(2σ) Ma and 615 ± 6 (2σ) Ma (Xu et al., 2009). The Tereeken diamictite is overlain by the Zhamoketi cap dolostone, which shares some sedimentary and geochemical features with the ~635 Ma Doushantuo cap dolostone in South China and other presumably correlative cap dolostones at the end of the Cryogenian Period (Xiao et al., 2004). The Hankalchough diamictite is <615 ± 6 (2σ) Ma (Xu et al., 2009) and lies below basal Cambrian phosphorites and cherts (Yao et al., 2005; Dong et al., 2009). Thus, the Hankalchough diamictite is clearly of Ediacaran age, and it may lie very close to the Ediacaran–Cambrian boundary (Shen et al., 2010).

The Hankalchough Formation can be lithologically divided into two members (Fig. 2). The lower diamictite member ranges from ~50 to ~400 m in thickness, representing glacial marine deposits. Out-sized clasts and dropstones in finely laminated facies are common. The Hankalchough diamictite member is overlain by the Hankalchough cap dolostone member, a 1–5 m thick unit of muddy-silty dolostone. Thin section observations indicate that the carbonate fraction of Hankalchough cap dolostone consists of homogenous dolomicrite and dolomicrosparite (Fig. 3). The content and grain size of siliciclastics (ranging from silt to clay sized particles) within the dolostone decrease upsection. Regionally, the Hankalchough diamictite has been correlated with the Hongtiegou glaciation in the Chaidam basin and the Luoquan glaciation in North China (Wang et al., 1980; Shen et al., 2007), but its correlation with other Ediacaran glaciations (e.g., the ~582 Ma Gaskiers glaciation in Newfoundland) is uncertain due to the lack of tight age constraints (Xiao, 2008). In this study, we sampled the Hankalchough cap dolostone at four sections: Yukkengol-North (YKG = Y′ in Fig. 1 of Xiao et al., 2004), Mochia-Khutuk (MK = M in Fig. 1 of Xiao et al., 2004), Hankalchough Peak (H = H′ in Fig. 1 of Xiao et al., 2004), and Zhaobishan (ZBS = H in Fig. 1 of Xiao et al., 2004).

The four investigated sections form a west–east lineation across the Quruqtagh basin arguably representing an onshore to offshore transect. This paleobathymetric interpretation is supported by several lines of sedimentological evidence. First, the Hankalchough diamictite thickens from

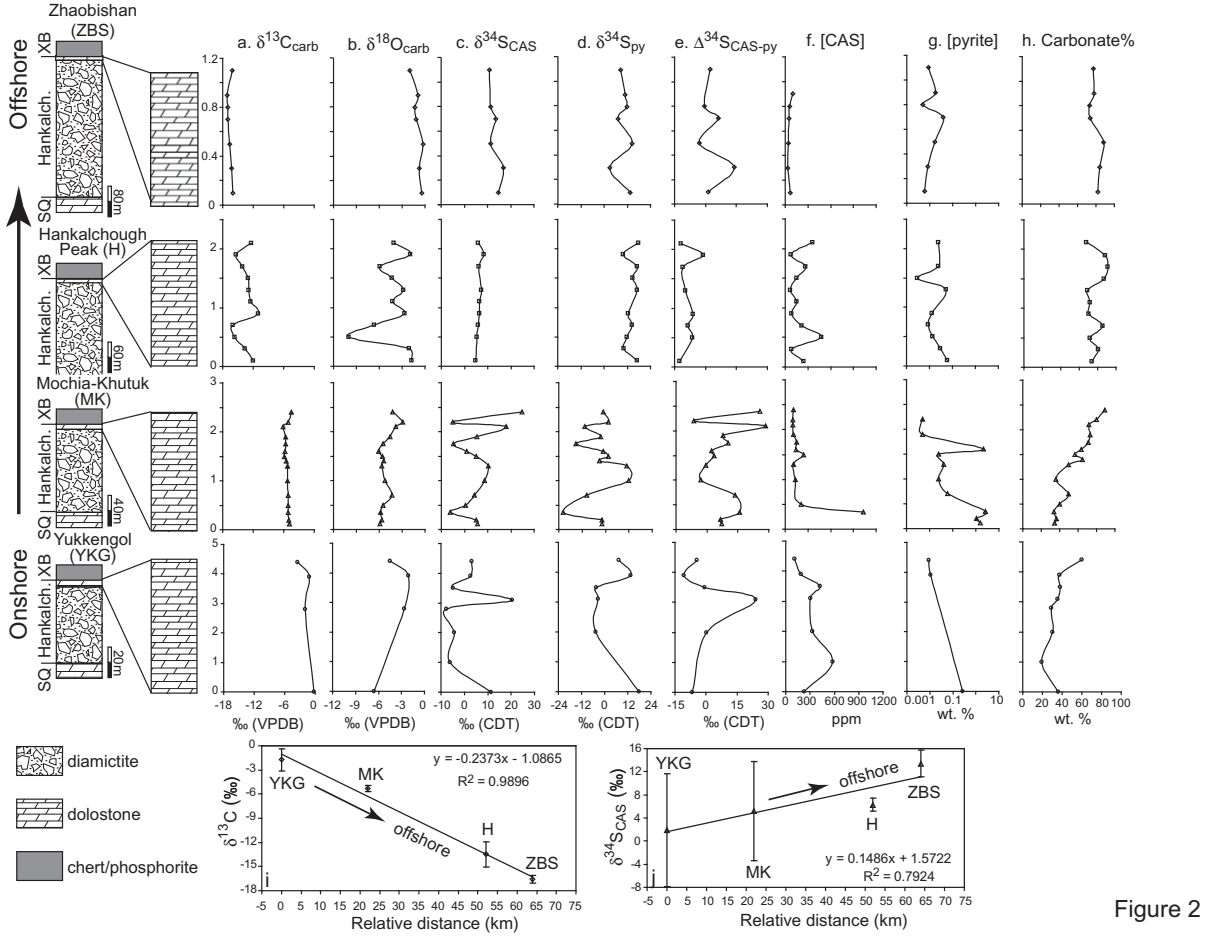

Figure 2

Fig. 2. Geochemical profiles of the four studied sections. (a) $\delta^{13}C$; (b) $\delta^{18}O$; (c) $\delta^{34}S_{CAS}$; (d) $\delta^{34}S_{py}$; (e) $\Delta^{34}S_{CAS-py} = \delta^{34}S_{CAS} - \delta^{34}S_{py}$; (f) CAS concentrations; (g) pyrite concentrations; (h) carbonate contents. (i and j) $\delta^{13}C_{carb}$ and $\delta^{34}S_{CAS}$ of the four studied section plotted against the relative distance between the sections. Symbols and brackets represent the average isotope values and one standard deviation, respectively, for each section. Linear regression lines, regression equations, and R values are shown. SQ: Shuiquan Formation; Hankalch: Hankalchough Formation; and XB: Xishanblaq Formation (basal Cambrian).

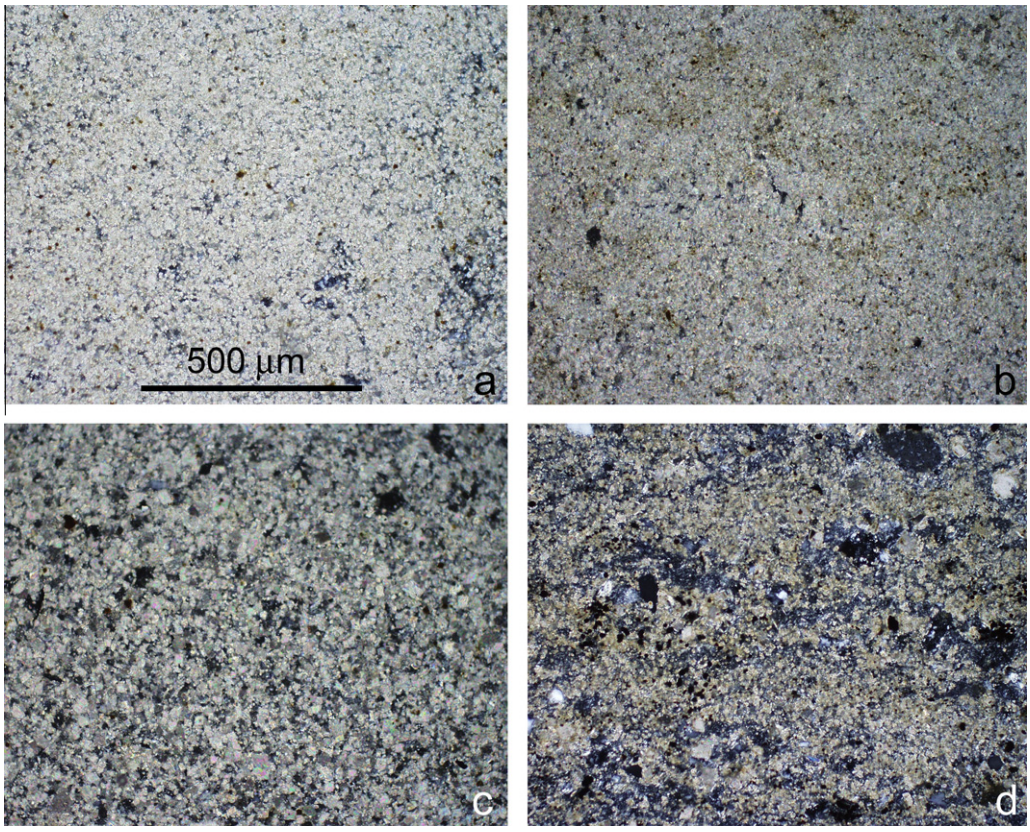

Fig. 3. Transmitted light photomicrographs of the Hankalchough cap dolostone at the four studied sections. (a) Zhaobishan (ZBS) section, homogenous microsparite, thin section ZBS-11; (b) Hankalchough Peak (H) section, homogenous micrite, thin section L-67; (c) Mochia-Khutuk (MK) section, homogenous microsparite, thin section MK-23; (d) Yukkengol-North (YKG) section, silty micrite, thin section YKG-59. Note the increasing detrital content from offshore (ZBS) to onshore (YKG) sections. Scale bar = 500 μm for all photomicrographs.

~50 m in the west to ~400 m in the east (Gao and Zhu, 1984), suggesting that the basin deepened to the east where more accommodation was provided for the rapid deposition of diamictite. Second, siliciclastic content and grain size (from silt to clay) in the Hankalchough cap carbonate decreases eastward and carbonate content shows a complementary increase (Fig. 2h), suggesting a terrigenous source from the west during the deposition of the cap dolostone. Third, a paleocurrent study of the underlying Zhamoketi Formation indicates a paleoflow direction from the southwest to the northeast (Li and Dong, 1991), consistent with the paleobathymetric trend of the Hankalchough Formation.

3. METHODS

$\delta^{13}C_{carb}$ and $\delta^{18}O_{carb}$ data and laboratory procedures were published in Xiao et al. (2004). In this study, we measured sulfur isotope compositions of carbonate associated sulfate (CAS) and pyrite, oxygen isotope composition of CAS, trace element concentrations (S, Mn, and Sr), and carbonate contents (carbonate%), using the same rock samples analyzed by Xiao et al. (2004). CAS extraction procedure was modified from Goldberg et al. (2005) and Shen et al. (2008). Fresh rock chips (30–50 g) were crushed to 80 mesh. Powders were repeatedly treated (>3 treatments and lasting >48 h) with 30% H_2O_2 to remove pyrite and organic matter. After the H_2O_2 treatments, powders were treated with 10% NaCl for 24 h to dissolve all non-CAS sulfate, and then were repeatedly (>3×) washed with deionized water. CAS was released by a step-wise acidification procedure that has been described in detail in Shen et al. (2008). Solution was passed through 1 μm filters to separate insoluble residues from the CAS bearing solutions. Insoluble residues were carefully washed, dried, and weighed to quantify carbonate content of samples. Supernatant was distributed into several centrifuge tubes, one of which was used for element analysis. Element concentrations were measured by inductively coupled plasma atomic emission spectroscopy (ICP-AES) at the Virginia Tech Soil Testing Laboratory, and calculated with insoluble residues subtracted from powder weight. CAS concentrations were determined from sulfur concentrations measured from ICP-AES analysis, again with insoluble residues subtracted from sample weight. Sulfate in the other centrifuge tubes was precipitated as barite by adding 1–2 ml of saturated $BaCl_2$ (30%) to each tube. Aliquots of barite precipitates were subsequently used for oxygen and sulfur isotope analyses.

Disseminated pyrite was extracted by a modified chromium reduction method (Canfield et al., 1986; Goldberg et al., 2005). Our extraction procedure was described in

detail by Shen et al. (2008). Pyrite concentrations were calculated from Ag_2S yields with insoluble residues subtracted from powder weight. Sulfur isotopes of $BaSO_4$ and Ag_2S precipitates were measured at University of Maryland on a GV Isoprime mass spectrometer, and are reported in the δ notation against V-CDT. Oxygen isotopes of $BaSO_4$ precipitates were analyzed at Louisiana State University Oxy-Anion Stable Isotope Center, and are reported in the δ notation against V-SMOW. Analytical uncertainties are 0.3‰ (1σ) and 0.5‰ (1σ) for sulfur and oxygen isotopes, respectively, and generally better than 5% for elements above detection limits.

4. RESULTS

Carbon and sulfur isotopic profiles from the four sections show substantial differences between our interpreted onshore and offshore sections. On average cap dolostone from offshore sections is depleted in ^{13}C and enriched in ^{18}O relative to the more siliciclastic rich nearshore sections (Tables 1 and 2; Fig. 2). Sulfur-34 abundances of both CAS and pyrite fractions are also enriched in the offshore sections relative to those nearer to the shoreline. Samples from the offshore sections show little variation in their *C*, *O*, and *S* isotope compositions. While the same is true for *C* and *O* isotopes in the onshore sections, ^{34}S abundances of both CAS and pyrite vary widely (Table 1). The onshore–offshore patterns in $\delta^{13}C_{carb}$ and $\delta^{34}S_{CAS}$ values are also shown in Fig. 2i and j, where the isotope data of each section are plotted against the present-day distance between the sections. Interestingly, there is a very good linear relationship between isotopes and distances, further supporting the paleobathymetry-dependent isotopic gradients in the Quruqtagh basin.

5. EVALUATION OF DIAGENETIC ALTERATION

Thin section observations indicate that the Hankalchough cap carbonate in all studied sections are composed of dolomicrite and dolomicrosparite with abundant terrigenous clay (particularly in the two onshore sections) and a small amount of disseminated pyrite (typically <0.1%). The fine grain size of the carbonate argues against high temperature alterations, which would result in extensive recrystallization and completely reset the isotopic systems. However, possible low temperature diagenetic alterations cannot be excluded on the basis of petrographic observations alone. Indeed the preservation of the cap carbonate as dolomicrite suggests some degree of alteration of the expected primary calcium carbonate sediments. Given the unusual environmental conditions that accompanied the Ediacaran ice ages, it is speculative but possible that these marine precipitates may have originally been dolomitic – rather than aragonitic – if shallow seawater became rapidly warmer, fresher (due to meltwater runoff), and lower in sulfate (cf. Fike et al., 2006; Ries et al., 2009) in the glacial aftermath. In this context we discuss the evidence for alteration revealed by the isotopic compositions of the Hankalchough cap dolostone.

Table 1
Summary of carbon, oxygen, and sulfur isotopic compositions of Hankalchough cap dolsotone in four sections.

Section	$\delta^{13}C_{carb}$ VPDB	$\delta^{18}O_{carb}$ VPDB	$\delta^{34}S_{CAS}$ VCDT	$\delta^{34}S_{py}$ VCDT
ZBS	-16.6 ± 0.5	-1.0 ± 0.6	$+13.4 \pm 2.3$	$+9.9 \pm 4.0$
H	-13.5 ± 1.6	-4.2 ± 2.5	$+6.3 \pm 1.1$	$+14.2 \pm 3.0$
MK	-5.3 ± 0.4	-5.1 ± 0.9	$+5.2 \pm 8.6$	-3.1 ± 9.0
YKG	-1.7 ± 1.4	-4.0 ± 2.1	$+1.9 \pm 9.8$	$+4.4 \pm 9.9$

5.1. Carbon isotopes

The diagenetic alteration of depositional $\delta^{13}C_{carb}$ values is controlled by the composition of diagenetic fluid and the mixing ratio between fluids and primary carbonates (Jacobsen and Kaufman, 1999; Knauth and Kennedy, 2009; Derry, 2010). Reaction of carbonates with meteoric water that is depleted in both ^{13}C and ^{18}O may lead to lower $\delta^{13}C_{carb}$ and $\delta^{18}O_{carb}$ values, resulting a positive correlation between $\delta^{13}C_{carb}$ and $\delta^{18}O_{carb}$, and the so-called "Forbidden Zone" where no marine carbonates reside (Knauth and Kennedy, 2009). It is notable that samples of the Hankalchough cap carbonate from the onshore sections (where meteoric diagenesis would be expected) fall within the lithification trend, whereas those from the offshore sections do not (Fig. 4a). These ^{13}C depleted samples are significantly enriched in ^{18}O with many delta values near to 0‰. Such values cannot be explained as falling off of the lithification trend solely by the process of dolomitization, insofar as at equilibrium authigenic dolomite would be enriched in ^{18}O by only ~2‰ relative to calcite at normal seawater temperatures (Kaufman et al., 1992).

Rather than reflecting diagenetic alteration, the overall array of Hankalchough samples forms a sub-vertical band on the carbon/oxygen crossplot that supports a perturbation of the global carbon cycle (cf. Knauth and Kennedy, 2009) in the aftermath of the ice age. Furthermore, it should be noted that diagenetic stabilization of marine carbonate by meteoric waters in these offshore sections is even more unlikely during post-glacial transgression. There is neither field evidence of methane seeps nor petrographic evidence for a gradient of increased alteration from offshore to onshore sections to support the view that methane oxidation resulted in the homogeneous carbon and oxygen isotope compositions of the offshore Hankalchough cap carbonate (Jiang et al., 2003; Wang et al., 2008).

Carbon isotope compositions of the Hankalchough cap dolostone also show a weak correlation with Mn/Sr (Fig. 4b) – an elemental monitor of meteoric alteration (Kaufman and Knoll, 1995), suggesting that the most negative $\delta^{13}C_{carb}$ values (around −16‰ at ZBS) are, in fact, the least altered. On the other hand, strontium isotope compositions in these dolomites vary between 0.710 and 0.720 (Xiao et al., 2004), which are inconsistent with $^{87}Sr/^{86}Sr$ values (ca. 0.7085) in well preserved limestone samples from broadly equivalent Ediacaran sections worldwide (Kaufman et al., 1993; Halverson et al., 2007). While these trace element measurements might also be taken as evidence for diagenetic alteration of carbon isotopes

Table 2
Geochemical data of the Hankalchough cap carbonate. The four sections (ZBS, H, MK, YKG) approximately represent an offshore-onshore transect. n.a.: not analyzed and n.s.: not sufficient yield.

Sample number	Height (m)	$\delta^{13}C$ (‰)	$\delta^{18}O$ (‰)	$\delta^{34}S_{py}$ (‰)	$\delta^{34}S_{CAS}$ (‰)	$\Delta^{34}S_{CAS}$ (‰)	$\delta^{18}O_{CAS}$ (‰)	$^{87}Sr/^{86}Sr$	Carbonate (%)	CAS (ppm)	Pyrite (%)	Mn/Sr
Section ZBS												
In contact with chert/phosphorite												
ZBS-4	1.4	n.a.	n.a.	n.a.	n.a.	n.a.	n.a.	n.a.	n.a.	n.a.	n.a.	n.a.
ZBS-5	1.3	n.a.	n.a.	n.a.	n.a.	n.a.	n.a.	n.a.	n.a.	n.a.	n.a.	2.39
ZBS-6	1.1	−16.2	−2.0	8.7	10.9	2.2	n.s.	0.7210362	77	n.s.	0.009	5.14
ZBS-7	0.9	−17.1	−0.9	10.7	n.s.	n.a.	n.s.	n.a.	78	102	0.018	6.22
ZBS-13	0.8	−17.0	−1.3	11.7	11.3	−0.4	n.s.	n.a.	73	61	0.005	4.68
ZBS-8	0.7	−16.9	−1.2	7.3	13.6	6.3	n.s.	0.7162001	74	54	0.038	3.85
ZBS-9	0.5	−16.6	−0.3	14.5	11.4	−3.1	n.s.	0.7137853	88	44	0.017	3.88
ZBS-10	0.3	−16.2	−0.8	2.8	16.8	14.0	n.s.	0.712973	84	35	0.008	n.a.
ZBS-11	0.1	−16.0	−0.4	13.4	14.8	1.4	n.s.	0.7138186	82	68	0.006	n.a.
In contact with Hankalchough diamictite												
Section H												
In contact with chert/phosphorite												
L-69	2.1	−12.3	−4.1	17.6	5.8	−11.8	7.7	n.a.	68	357	0.024	2.41
L-68	1.9	−15.4	−1.9	9.7	8.5	−1.2	n.s.	0.7200232	88	78	n.s.	2.04
L-67	1.7	−14.1	−5.9	17.0	6.1	−10.9	n.s.	n.a.	91	271	0.024	2.22
L-66	1.5	−12.9	−4.4	14.9	n.s.	n.a.	n.s.	0.720492	87	154	0.003	2.66
L-65	1.3	−12.9	−2.8	17.0	7.2	−9.8	n.s.	n.a.	69	70	0.053	3.95
L-64	1.1	−12.5	−4.2	n.a.	6.5	n.a.	n.s.	0.7198593	71	148	n.a.	3.57
L-63	0.9	−11.0	−2.6	12.5	6.4	−6.1	n.s.	n.s.	70	86	0.013	4.52
L-73	0.7	−15.9	−6.7	14.4	6.0	−8.4	n.s.	0.7193278	85	214	0.009	2.04
L-72	0.5	−15.6	−10.0	11.7	5.4	−6.3	7.4	0.7215158	72	482	0.014	3.85
L-71	0.3	−13.6	−2.1	10.3	n.s.	n.s.	n.s.	n.a.	81	86	0.029	5.26
L-70	0.1	−12.1	−1.8	17.2	4.7	−12.5	n.s.	0.7199831	74	243	0.061	5.47
In contact with Hankalchough diamictite												
Section MK												
In contact with chert/phosphorite												
MK-28	2.4	−4.5	−4.2	−1.0	24.7	25.7	n.s.	0.711508	89	108	n.a.	6.75
MK-26	2.2	−5.1	−2.9	1.5	−5.0	−6.5	n.s.	0.713296	80	105	0.005	5.79
MK-25	2.1	−6.1	−3.8	−10.6	17.9	28.4	n.s.	0.713156	72	101	n.a.	6.93
MK-24	1.9	−5.6	−4.6	−2.4	5.5	7.9	9.3	0.715191	73	108	0.005	6.67
MK-23	1.75	−5.6	−5.5	−15.1	−4.8	10.3	n.s.	n.a.	71	150	n.a.	4.99
MK-22	1.6	−5.8	−6.1	−1.3	0.9	2.2	n.s.	n.a.	64	142	2.091	4.12
MK-21	1.5	−5.9	−5.6	1.5	5.0	3.5	8.1	0.715947	57	243	0.025	4.88
MK-20	1.4	−5.6	−5.4	−3.0	n.s.	n.a.	n.s.	n.a.	65	n.s.	n.a.	n.a.
MK-19	1.3	−5.2	−5.7	10.8	10.3	−0.5	n.s.	0.716664	50	105	0.04	4.30
MK-18	1	−5.2	−5.2	11.8	8.8	−3.1	n.s.	n.a.	36	137	0.025	4.10
MK-17	0.7	−5.2	−4.4	−9.6	4.1	13.7	n.s.	0.715433	50	n.s.	0.059	n.a.
MK-16	0.5	−5.1	−5.5	n.a.	0.4	n.a.	6.6	n.a.	40	209	n.a.	4.62
MK-15	0.35	−5.1	−5.9	−21.8	−6.1	15.7	6.3	0.716742	34	1032	2.603	4.08
MK-14	0.2	−5.0	−5.6	−1.7	5.0	6.7	n.s.	0.716679	37	n.s.	1.067	n.a.

MK-13	0.12	−4.9	−5.9	−1.8	5.5	7.3	8.4	0.716777	34	n.s.	1.582	n.a.
In contact with mudstone and diamictite												
Section YKG												
In contact with chertlphosphorite												
YKG-61	4.8	n.a.	n.a.	n.a.	n.a.	n.a.	n.a.	n.a.	n.a.	n.a.	n.a.	5.12
YKG-60	4.4	−3.5	−4.5	7.5	3.0	−4.5	n.s.	n.a.	60	111	0.009	7.49
YKG-59	3.9	−1.2	−2.1	13.4	2.8	−10.6	7.8	0.7103803	38	189	0.011	12.12
YKG-58	3.5	n.a.	n.a.	−4.3	−4.8	−0.5	7.6	n.a.	38	425	n.a.	6.74
YKG-57	3.1	n.a.	n.a.	−3.3	20.5	23.9	7.9	n.a.	35	306	n.a.	n.a.
YKG-56	2.8	−2.0	−2.6	n.a.	−7.7	n.a.	4.2	n.a.	29	n.s.	n.a.	16.64
YKG-55	2	n.a.	n.a.	−4.5	−4.3	0.3	5.1	n.a.	30	328	n.a.	11.76
YKG-54	1	n.a.	n.a.	n.a.	−6.1	n.a.	n.s.	n.a.	19	577	n.a.	4.83
YKG-53	0	−0.2	−6.6	17.9	11.3	−6.6	n.s.	0.7108137	36	229	0.27	5.12
In contact with Hankalchough diamictite												

(Kaufman and Knoll, 1995), it is more likely that the strontium isotopic compositions of these dolomites (known to typically preserve less Sr than their calcitic or aragonitic equivalents) were affected by the radiometric decay of ^{87}Rb from the abundant clays observed in thin section and as insoluble residues, with little impact on $\delta^{13}C$ or $\delta^{18}O$ values of the rock.

5.2. Sulfur isotopes

Carbonate associated sulfate (CAS) is trace sulfate that substitutes for CO_3^{2-} during carbonate precipitation (Pingitore et al., 1995). General agreement between $\delta^{34}S_{CAS}$ and seawater $\delta^{34}S_{sulfate}$ (within a few per mil) has been observed in both modern and ancient carbonates (Burdett et al., 1989; Kah et al., 2004), suggesting that $\delta^{34}S_{CAS}$ can be broadly used as a proxy for seawater $\delta^{34}S_{sulfate}$ compositions (Kampschulte et al., 2001; Kampschulte and Strauss, 2004). However, possible diagenetic alterations of $\delta^{34}S_{CAS}$ should be carefully evaluated, particularly for dolomite samples. Recent analyses of intercalated dolomite and evaporate samples from the Mesoproterozoic Society Cliff Formation dolostone reveals similar (within 4‰) $\delta^{34}S$ values (Kah et al., 2004; Fike and Grotzinger, 2010). The same is revealed for CAS sulfur isotopes in Triassic dolostones and evaporates, but these are slightly depleted in ^{34}S (by a few permil) relative to the correlative limestones in more offshore environments (Marenco et al., 2008b). The reason for such discrepancy is unknown, but broad similarities in $\delta^{34}S$ values between dolostones and intercalated evaporate, and limestone samples from temporally equivalent facies suggest that any of these lithotypes may be used as proxies for ancient seawater.

The sulfur isotopic composition of ancient samples is also subject to contamination from gypsum dissolution or pyrite oxidation during laboratory extraction. Non-structurally bound sulfate (e.g. gypsum) is generally removed by repetitive treatment of powdered samples with NaCl or H_2O_2 leaching solutions followed by repeated washing with deionized water (Goldberg et al., 2005). We suggest that the leaching step should be repeated until no $BaSO_4$ precipitate is observed in the sequential leachates after addition of $BaCl_2$. Such tests may reveal the presence of sulfate formed by the oxidation of pyrite at the outcrop. On the other hand, pyrite oxidation during laboratory preparations may also result in anomalous $\delta^{34}S_{CAS}$ values, particularly in samples enriched with both pyrite and reactive Fe^{3+} (Marenco et al., 2008a,b; Mazumdar et al., 2008).

Several lines of evidence indicate that our $\delta^{34}S_{CAS}$ data are not biased by pyrite oxidation. First, most samples have very low pyrite concentration (<0.1 wt.%) as determined by Ag_2S yields (Table 2, Fig 2g). In order to minimize the potential effect of pyrite oxidation, we pretreated sample powders with 30% H_2O_2 (>3 times) until no discernable bubbles were produced to quantitatively remove pyrite. We suggest that the lack of correlation between $\delta^{34}S_{CAS}$ and [CAS] (Fig. 4c), between $\delta^{34}S_{CAS}$ and pyrite% (Fig. 4d), and between $\delta^{34}S_{CAS}$ and $\delta^{34}S_{py}$ (Fig. 4e) argue against significant contamination by pyrite oxidation. Finally, negative fractionations between CAS and pyrite (i.e., $\delta^{34}S_{CAS} < \delta^{34}S_{py}$;

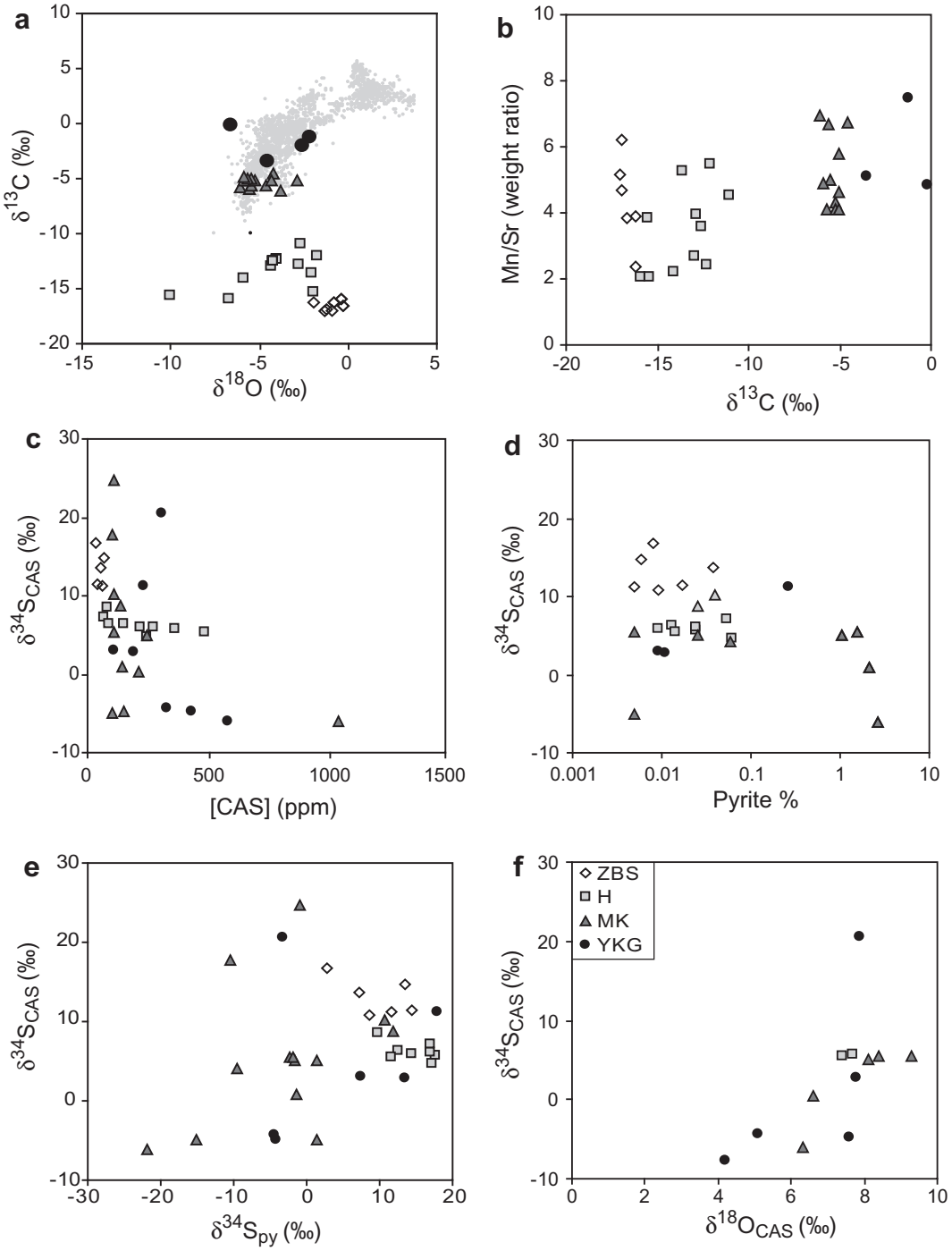

Fig. 4. Isotope and elemental cross-plot. (a) $\delta^{18}O_{carb}$ vs. $\delta^{13}C_{carb}$, the shadowed area is the reference domain from Knauth and Kennedy, 2009, indicating the lithification trend of marine carbonates; (b) $\delta^{13}C_{carb}$ vs. Mn/Sr; (c) $\delta^{34}S_{CAS}$ vs. [CSA]; (d) $\delta^{34}S_{CAS}$ vs. [pyrite]; (e) $\delta^{34}S_{CAS}$ vs. $\delta^{34}S_{py}$; and (f) $\delta^{34}S_{CAS}$ vs. $\delta^{18}O_{CAS}$.

Fig. 2e) in many samples are also inconsistent with contamination from *in situ* pyrite oxidation.

Pyrite in the Hankalchough cap dolostone is preserved as disseminated microcrystals mostly between 5 and 10 μm in size (Fig. 3). These grains were probably formed either in an anoxic water column (syngenetic pyrites) or within shallow depth of sediments. Thus, $\delta^{34}S_{py}$ values may reflect isotopic compositions of seawater or pore waters that were ultimately derived from seawater.

To summarize, although diagenetic processes may have had an overprint on the $\delta^{13}C_{carb}$ and $\delta^{34}S_{CAS}$ values of some samples, the distinct spatial pattern cannot be explained by diagenetic alteration alone. Instead, we suggest that this pattern may represent a spatial geochemical

gradient and offers an opportunity to constrain the geochemical conditions in the Quruqtagh basin after the Ediacaran Hankalchough glaciation. Below, we use a mixing model involving three end members (surface water, deep-basin water, and terrestrial weathering input) to further constrain the environmental conditions in the aftermath of an Ediacaran ice age.

6. POSTGLACIAL GEOCHEMICAL GRADIENT AND PARTIAL MIXING

Isotopic data of the Hankalchough cap dolostone have two characteristic features: (1) $\delta^{13}C_{carb}$ values are extremely low in two offshore sections and become more positive toward onshore, and (2) $\delta^{34}S_{CAS}$ values of the two onshore sections are more variable but generally lower than those of the two offshore sections, although overall the Hankalchough values are lower than values reported from other Ediacaran marine carbonates (Fike et al., 2006; McFadden et al., 2008; Ries et al., 2009). Considering the paleobathymetric trend of the Quruqtagh basin, the onshore–offshore $\delta^{13}C_{carb}$ gradient can be interpreted in terms of mixing between marine surface water and ^{13}C-depleted deep-basin water. As for the sulfur isotopes, comparatively lower $\delta^{34}S_{CAS}$ values in the onshore sections likely reflect incorporation of ^{34}S-depleted sulfate derived from terrestrial weathering of sedimentary sulfides. Thus, the geochemical data of the Hankalchough cap dolostone can be interpreted in terms of a partial mixing of three end members: surface water (S), deep-basin water (D), and terrestrial weathering input (T). Below, we explore some quantitative calculations to place constraints on this mixing model.

6.1. Model description

We use a three-component mixing model to evaluate the relative contributions of each component. In this model, $\delta^{13}C_{carb}$ and $\delta^{34}S_{CAS}$ values of the Hankalchough cap dolostone are determined by the proportional mixing of the three components:

$$\delta^{13}C_{carb} = \frac{(\delta^{13}C_{surf} \times F_{surf} \times m^{C}_{surf} + \delta^{13}C_{deep} \times F_{deep} \times m^{C}_{deep} + \delta^{13}C_{terr} \times F_{terr} \times m^{C}_{terr})}{(F_{surf} \times m^{C}_{surf} + F_{deep} \times m^{C}_{deep} + F_{terr} \times m^{C}_{terr})} \quad (1)$$

$$\delta^{34}S_{CAS} = \frac{(\delta^{34}S_{surf} \times F_{surf} \times m^{S}_{surf} + \delta^{34}S_{deep} \times F_{deep} \times m^{S}_{deep} + \delta^{34}S_{terr} \times F_{terr} \times m^{S}_{terr})}{(F_{surf} \times m^{S}_{surf} + F_{deep} \times m^{S}_{deep} + F_{terr} \times m^{S}_{terr})} \quad (2)$$

where F_i represents water masses in component i, which should be the same for both carbon and sulfur systems, and m^{C}_{i} and m^{S}_{i} denote, respectively, the DIC and sulfate concentrations in component i. The subscripts surf, deep, and terr represent the surface water, deep-basin water, and terrestrial weathering input, respectively. For simplicity, we define $M^{C}_{i} = F_i \times m^{C}_{i}$ and $k_i = m^{S}_{i}/m^{C}_{i}$. To calculate the relative contributions of DIC in the three components, we set the denominator in the right side of Eq. (1) to be unity, i.e. $M^{C}_{surf} + M^{C}_{deep} + M^{C}_{terr} = 1$. Therefore, M^{C}_{i} now becomes the fraction of DIC from component i, and k_i describes the concentration ratio between sulfate and DIC in component i. The Eqs. (1) and (2) can be rewritten as:

$$\delta^{13}C_{carb} = \delta^{13}C_{surf} \times M^{C}_{surf} + \delta^{13}C_{deep} \times M^{C}_{deep} + \delta^{13}C_{terr} \times M^{C}_{terr} \quad (3)$$

$$\delta^{34}S_{CAS} = \frac{(\delta^{34}S_{surf} \times k_{surf} \times M^{C}_{surf} + \delta^{34}S_{deep} \times k_{deep} \times M^{C}_{deep} + \delta^{34}S_{terr} \times k_{terr} \times M^{C}_{terr})}{(k_{surf} \times M^{C}_{surf} + k_{deep} \times M^{C}_{deep} + k_{terr} \times M^{C}_{terr})} \quad (4)$$

We can also calculate the relative contributions of sulfate in the three components by setting the denominator in the right side of Eq. (2) to be unity, i.e. $M^{S}_{surf} + M^{S}_{deep} + M^{S}_{terr} = 1$, where M^{S}_{i} represents the proportion of sulfate from component i. Thus, Eqs. (1) and (2) can be written as:

$$\delta^{13}C_{carb} = \frac{(\delta^{13}C_{surf} \times M^{S}_{surf}/k_{surf} + \delta^{13}C_{deep} \times M^{S}_{deep}/k_{deep} + \delta^{13}C_{terr} \times M^{S}_{terr}/k_{terr})}{(M^{S}_{surf}/k_{surf} + M^{S}_{deep}/k_{deep} + M^{S}_{terr}/k_{terr})} \quad (5)$$

$$\delta^{34}S_{CAS} = (\delta^{34}S_{surf} \times M^{S}_{surf} + \delta^{34}S_{deep} \times M^{S}_{deep} + \delta^{34}S_{terr} \times M^{S}_{terr}) \quad (6)$$

In this model, we assume that the surface water had a DIC concentration (m^{C}_{surf}) of 2 mM and a DIC carbon isotope composition ($\delta^{13}C_{surf}$) of ~0‰, both of which are comparable to the modern surface ocean chemistry. We further assume that the sulfur isotope composition of surface water sulfate ($\delta^{34}S_{surf}$) was +20‰, which is close to the

modern seawater composition as well. There is no constraint on the surface water sulfate concentration (m^S_{surf}), but as shown below m^S_{surf} can be constrained by deep-basin water chemistry ($m^S_{deep}, m^C_{deep}, \delta^{34}S_{deep}$, and $\delta^{13}C_{deep}$).

To parameterize the deep-basin water component, we follow earlier studies that suggest Ediacaran deep oceans were probably anoxic (Canfield et al., 2008) and enriched in dissolved organic carbon (DOC) (Rothman et al., 2003; Swanson-Hysell et al., 2010). Remineralization of DOC in anoxic deep oceans by anaerobic sulfate reduction bacteria would generate ^{12}C-enriched DIC. The relative abundance of pre-existing DIC vs. regenerated DIC through deep-basin DOC remineralization determines the carbon isotope composition of the deep water component ($\delta^{13}C_{deep}$). In modern deep oceans, DIC (2 mM) is about ~50 times more abundant than DOC (42 μM) (Eglinton et al., 2003). In anoxic Ediacaran deep oceans (Canfield et al., 2008), a larger amount of DOC can be assumed (Rothman et al., 2003; Swanson-Hysell et al., 2010), although there is no consensus about exact concentrations. As a possible modern analog to the Ediacaran Ocean, we use Pony Lake in the Antarctica; the Pony Lake ecosystem is exclusively composed of bacteria and algae without the presence of any metazoans. In Pony Lake, DOC concentration is up to 8 mM (Dieser et al., 2006). Thus, it is plausible to accumulate DOC in levels several times higher than that of DIC in an anoxic Neoproterozoic deep basin when animals (particularly zooplankton that are critical in maintaining a Phanerozoic style carbon cycle; (Logan et al., 1995)) were ecologically unimportant. In an anoxic deep ocean (Canfield et al., 2008), remineralization of DOC is mostly carried out by anaerobic bacteria, primarily by sulfate reducing bacteria. Bacterial sulfate reduction can be approximated by the following reaction:

$$SO_4^{2-} + 2CH_2O = H_2S + 2HCO_3^- \quad (7)$$

As shown in Eq. (7), one mole of sulfate oxidizes two moles of organic carbon. If the deep-basin water was anoxic and ferruginous (Canfield et al., 2008), ^{32}S-enriched sulfide derived from bacterial sulfate reduction would have been quantitatively precipitated as pyrite (i.e., no reoxidation of H_2S when deep water was upwelled onto shallow shelves). Thus, the remaining sulfate in deep basin was enriched in ^{34}S. If we assume that there was sufficient supply of sulfate relative to DOC availability, a mass balance equation can be written.

$$\delta^{34}S_{deep0} \times m^S_{deep0} = \delta^{34}S_{deep} \times (m^S_{deep0} - m_{DOC}/2) + \delta^{34}S_{pyrite} \times m_{DOC}/2 \quad (8a)$$

where m^S_{deep0} and $\delta^{34}S_{deep0}$ are the initial (before remineralization) concentration and isotopic composition of deep-basin sulfate, $\delta^{34}S_{deep}$ is sulfate sulfur isotopic composition after remineralization, $\delta^{34}S_{pyrite}$ is sulfur isotopic composition of cumulative pyrite product, and m_{DOC} is the amount of DOC (expressed as DOC concentration) that is remineralized to HCO_3^-. Thus, $\delta^{34}S_{deep}$ can be solved as follows:

$$\delta^{34}S_{deep} = \delta^{34}S_{deep0} - \Delta \times \left(\frac{m_{DOC}}{2 \times m^S_{deep0}}\right) \quad (8b)$$

where $\Delta = \delta^{34}S_{pyrite} - \delta^{34}S_{residual\ sulfate}$, defined as the isotopic difference between pyrite produced by bacterial sulfate reduction and the residual sulfate in deep basin water. Note that this definition is different from the fractionation associated with bacterial sulfate reduction, which is typically defined as $\Delta^{34}S = \delta^{34}S_{initial\ sulfate} - \delta^{34}S_{pyrite}$ or $\delta^{34}S_{CAS} - \delta^{34}S_{py}$.

To simplify our model, we also assume that the Quruqtagh basin was originally well mixed and stratification happened as a result of basin restriction/isolation during glacioeustatic sea-level fall. At the initiation of stratification, the deep-basin water and surface water had identical compositions in both DIC and sulfate, i.e. $m^S_{deep0} = m^S_{surf}$ and $\delta^{34}S_{deep0} = \delta^{34}S_{surf}$. Convective mixing of sulfate and DIC between the surface and deep-basin water was then shut off by basin stratification. Thus, Eq. (8b) can be written as:

$$\delta^{34}S_{deep} = \delta^{34}S_{surf} - \Delta \times \left(\frac{m_{DOC}}{2 \times m^S_{surf}}\right) \quad (9)$$

Similarly, a mass balance equation can be written for the carbon system and $\delta^{13}C_{deep}$ can be determined as follows:

$$\delta^{13}C_{deep} = \frac{(\delta^{13}C_{surf} \times m^C_{surf} + \delta^{13}C_{DOC} \times m_{DOC})}{(m^C_{surf} + m_{DOC})} \quad (10)$$

where $\delta^{13}C_{DOC}$ is the isotopic composition of DOC in deep-basin water.

In order to couple the carbon and sulfur cycles, we define two new parameters: $\alpha = m_{DOC}/m^C_{surf}$ and $\beta = 0.5 \times m_{DOC}/m^S_{surf}$. α denotes the remineralized DOC concentration in deep-basin water relative to surface water DIC concentration. For example, the maximum α for the modern ocean is ~0.02 when all DOC is quantitatively remineralized to DIC. In contrast, in Pony Lake, the α value can be up to 4 (with [DOC] = 8 mM and [DIC] = 2 mM).

In this analysis β can be understood in two ways. First, it describes the ratio between the remineralized deep-basin DOC concentration and surface water sulfate concentration, and gives an estimate about the sulfate availability during anaerobic oxidation of DOC. Second, β is the fraction of sulfate reduction in deep-basin water. Given the consensus of generally low sulfate concentration in Neoproterozoic ocean, essentially all marine sulfur was reduced and buried as pyrite (Canfield and Raiswell, 1991), i.e. β should be close to 1. In our simulation, we choose $\alpha = 3$ and $\beta = 0.9$. Assuming $\delta^{13}C_{DOC} = -30‰$, $m^C_{surf} = 2$ mM, $\delta^{13}C_{surf} = 0‰$, $\delta^{34}S_{surf} = 20‰$, and $\Delta = -20‰$, m^C_{deep}, m^S_{surf}, m^S_{deep}, $\delta^{13}C_{deep}$, and $\delta^{34}S_{deep}$ are calculated as 8 mM, 3.3 mM, 0.3 mM, −22.5‰, and +38‰, respectively. With the above assumed values, the cumulative $\delta^{34}S_{pyrite}$ produced in the deep-basin water is ~+18‰; this value is close to the upper bound of $\delta^{34}S_{pyrite}$ of the Hankalchough cap dolostone in the two offshore sections (+2.8‰ to +17.6‰ with average of +12.5 ± 4‰).

Terrestrial weathering input forms another important end-member in our model. The carbon and sulfur isotope compositions of the weathering input ($\delta^{13}C_{terr}$ and $\delta^{34}S_{terr}$) strongly depend on the lithologies of the source region, and are difficult to constrain. In our model, we use the modern $\delta^{13}C_{terr}$ value of −6‰ (Schrag et al., 2002). To capture the full range of Hankalchough $\delta^{34}S_{CAS}$ values (between

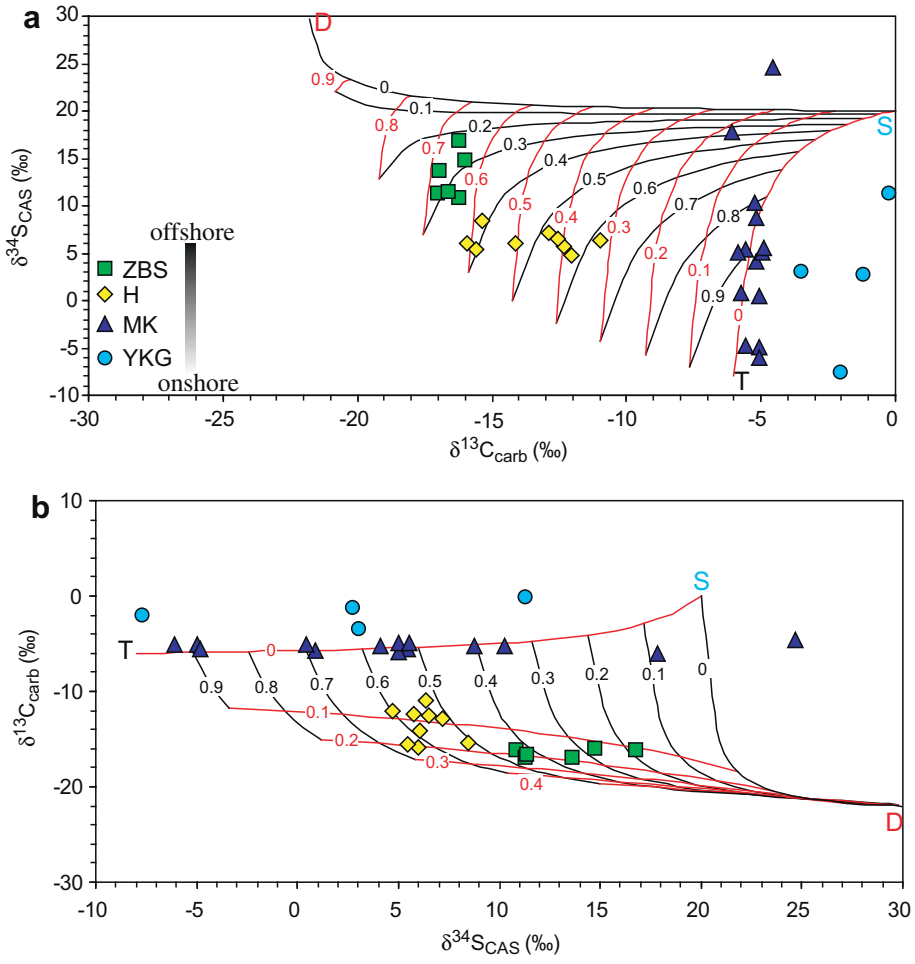

Fig. 5. (a) A $\delta^{13}C_{carb} - \delta^{34}S_{CAS}$ space plotted using the mixing model of the carbon system (Eqs. (3) and (4); assuming total DIC input to be unity). (b) A $\delta^{34}S_{CAS} - \delta^{13}C_{carb}$ space plotted using the mixing model of the sulfur system (equations, not shown in text, are similar to Eqs. (3) and (4); assuming total sulfate input to be unity). The two plots are similar. Red contour lines represent the fraction of deep-basin water component, and black contour lines represent the fraction of terrestrial weathering input. D, S, and T denote the corner where the deep-ocean water, surface-ocean water, and terrestrial weathering input dominates. ZBS: Zhaobishan section; H: Hankalchough Peak section; MK: Mochia-Khutuk section; and YKG: Yukkengol-North section.

−7.7‰ and 24.7‰), we choose a $\delta^{34}S_{terr}$ value of −8‰, which is lower than the globally averaged modern value of +6‰ (Kah et al., 2004). The choice of $\delta^{34}S_{terr} = -8‰$ does not represent a global value during the Ediacaran Period, but an estimate of the local terrestrial sulfate input to the Quruqtagh basin. This estimate is justified by the $\delta^{18}O_{CAS}$ data: the positive correlation between $\delta^{34}S_{CAS}$ and $\delta^{18}O_{CAS}$ (Fig. 4f), in which the lowest $\delta^{34}S_{CAS}$ (−7.7‰) corresponds to the lowest $\delta^{18}O_{CAS}$ value of ~+4‰. Sulfate derived from sulfide (e.g., pyrite) oxidation, either biotic or abiotic, is characterized by low $\delta^{18}O$ values; this is because oxygen in such sulfate is mainly derived from ^{18}O depleted water–oxygen rather than ^{18}O-enriched molecular-oxygen (Balci et al., 2007). Post-depositional pyrite oxidation (e.g. oxidation during outcrop weathering or laboratory CAS extraction) is not the cause for low $\delta^{18}O_{CAS}$ values as indicated by the inverse fractionation between CAS and pyrite (Fig. 2e). Neither could the low $\delta^{18}O_{CAS}$ values result from exchange between sulfate–oxygen and water–oxygen, because such reaction is extremely slow even under low pH conditions (Chiba and Sakai, 1985). Thus, the only currently viable interpretation is that significant amount of CAS, particular in samples with low $\delta^{18}O_{CAS}$ values, was derived from oxidative weathering of pyrite from terrestrial input. $\delta^{18}O$ of modern river water sulfate varies between −2‰ and +5‰, in sharp contrast to the oxygen isotopic composition of modern marine sulfate of ~+9‰ (Van Stempvoort and Krouse, 1994). The lowest $\delta^{18}O_{CAS}$ value observed in the Hankalchough cap dolostone is +4‰, approaching the upper bound of modern riverine sulfate. Assuming Ediacaran riverine sulfate has a $\delta^{18}O$ range similar to modern values, $\delta^{34}S_{CAS}$ of samples with the lowest $\delta^{18}O_{CAS}$ values can be used as a maximum estimate of sulfur isotopic composition of riverine sulfate in the Quruqtagh basin. Thus, we choose −8‰ as a representative value for the local source of sulfate from terrestrial oxidative weathering of pyrites.

The concentrations of terrestrial weathering input of DIC (m^C_{terr}) and sulfate (m^S_{terr}) are difficult to determine, but we can estimate the possible DIC/sulfate ratios (C/S).

C/S ratios of modern rivers vary between ~1 and 100, and rivers draining from siliciclastic source areas have (C/S) ratios between 3 and 5 (Meybeck et al., 2003). If most terrestrial sulfate was derived from pyrite oxidation, the C/S ratio of terrestrial input should be close to that of rivers draining from siliciclastic source areas. Here, we choose (C/S) ratio of 5, the upper bound for rivers draining through siliciclastic regions.

6.2. Modeling result

The relative contributions of D, S, and T to the Hankalchough cap dolostone can be evaluated by the mixing model (Fig. 5). Except for the YKG section, the measured carbon and sulfur isotopes of the three other sections all fall within the range predicted by the mixing model. The distribution of the sections within the $\delta^{13}C_{carb}$–$\delta^{34}C_{CAS}$ space is consistent with their paleobathymetric location along an onshore–offshore transect, and much of the isotopic variations between the sections can be explained by the relative input from D and T.

$\delta^{13}C_{carb}$ values are strongly affected by the deep-basin input because of its high DIC contents and extreme $\delta^{13}C$ values. In the two offshore sections, deep-basin water may have contributed 60–70% (ZBS section) and 40–60% (H section) of DIC for the cap dolostone precipitation, whereas it probably made very little contribution to carbonate precipitation at the onshore MK section. On the other hand, terrestrial input has the highest impacts on cap carbonate precipitation at MK (>80%), but accounts for 40–60% and 20–30% DIC for cap carbonate precipitation at H and ZBS sections, respectively. Surface water has little contribution for all sections (<20%), probably because the surface water was volumetrically small and DIC-poor relative to deep water in the Quruqtagh basin.

On the other hand, the model suggests that deep-basin sulfate accounts for less than 20% of sulfate for all sections, probably because of its very low sulfate concentrations (Li et al., 2010). About 10–40% and 50% of sulfate in the offshore sections at ZBS and H comes from terrestrial input. This result also explains the generally lower $\delta^{34}S_{CAS}$ values of the Hankalchough cap dolostones relative to values from other Ediacaran marine carbonates. In the onshore MK section, $\delta^{34}S_{CAS}$ values are highly variable. We speculate that the variation in $\delta^{34}S_{CAS}$ may reflect low sulfate concentration in seawater, under which conditions both sulfate concentration and $\delta^{34}S_{sulfate}$ are susceptible to external perturbations. For example, short term variations in terrestrial influx of sulfate might have had significant effect on $\delta^{34}S_{sulfate}$. Compared with the MK section, the offshore sections at ZBS and H have less stratigraphic variation in $\delta^{34}S_{CAS}$, although terrestrial inputs still contribute 10–50% of sulfate. We speculate that the lack of significant stratigraphic variation of $\delta^{34}S_{CAS}$ in two offshore sections were the result of sufficient mixing between terrestrial and oceanic sulfate, which eliminates the short term variation in terrestrial input of sulfate.

We notice that most YKG samples are plotted outside the field predicted by the mixing model (Fig. 5). There are two possibilities. Either the YKG isotopic signatures have been diagenetically altered, or some variables in the mixing model were improperly parameterized. In particular, we used the modern values of $\delta^{13}C_{surf}$ and $\delta^{13}C_{terr}$ in the modeling. Whereas our model is not sensitive to $\delta^{13}C_{surf}$, a slight increase in $\delta^{13}C_{terr}$ would accommodate the YKG data in the predicted field. This suggests that, like the sulfur system, isotopic values of the terrestrial input to the Quruqtagh basin may reflect local or regional conditions, and can be different from the global average.

6.3. Sensitivity test

In our model, $\delta^{13}C_{surf}$, $\delta^{34}S_{surf}$, $\delta^{13}C_{terr}$, and m^{C}_{surf} are assigned to the modern values. $\delta^{34}S_{terr}$ is given a value that departs from the modern global average but may be pertinent to the Quruqtagh basin as indicated by the $\delta^{18}O_{CAS}$ values (Fig. 4f). m^{C}_{terr} and m^{S}_{terr} are unknown, but the C/S ratio is given a modern value for rivers draining through siliciclastic regions. In addition to these parameters, there are three variables α, β, and Δ that are loosely constrained.

Keeping other factors constant, any variation in α, β, or Δ will change the model results. The sensitivity of the model results to variations in α, β, and Δ is shown in Fig. 6. In a $\delta^{13}C$ vs. $\delta^{34}S$ plot, any $\delta^{13}C$ and $\delta^{34}S$ pairs that can be interpreted by the mixing model should be plotted within a triangular area, which is defined by three mixing lines: mixing between surface water and deep-basin water, surface water and terrestrial weathering input, and deep-basin water and terrestrial whether input. Isotopic data that plot outside the triangles cannot be explained by the mixing model (either due to diagenetic alteration of the isotopic signatures or due to incorrect parameterization). As shown in Fig. 6, to accommodate the data, α must be $\geqslant 2$ (Fig. 6a), i.e. the remineralized DOC must be greater than 4 mM, which is twice the modern ocean DIC concentration of 2 mM and ~100 times the model DOC level. This is not unreasonable given the DOC concentration of 8 mM in Pony Lake. Likewise, β should be no less than 0.85 (Fig. 6b) to accommodate the measured data, suggesting that >85% of sulfate in deep-basin water has been used to remineralize DOC. Fig. 6c shows that the model is insensitive to the magnitude of Δ, which ranges from $-20‰$ to $-45‰$.

The mixing model also implicitly requires that the isotopic gradients in the Quruqtagh basin was maintained on the time scale represented by the cap dolostone precipitation, perhaps 1000–100,000 years (Hyde et al., 2000; Hoffman et al., 2007). Such gradients can be kinetically sustained on a similar time scale by the strong terrestrial weathering input and/or upwelling from deep-basin water in the aftermath of the Hankalchough glaciation. In fact, empirical data (Li et al., 2010) and geochemical modeling (Johnston et al., 2009) suggest that oceanic anoxia and euxinia can be maintained for millions of years when atmospheric pO_2 level was low.

6.4. Interpretation of inverse fractionation in sulfur isotope

Perhaps the most enigmatic feature of the Hankalchough cap dolostone is that 17 out of the 33 samples (including all four sections) showing inverse sulfur isotope

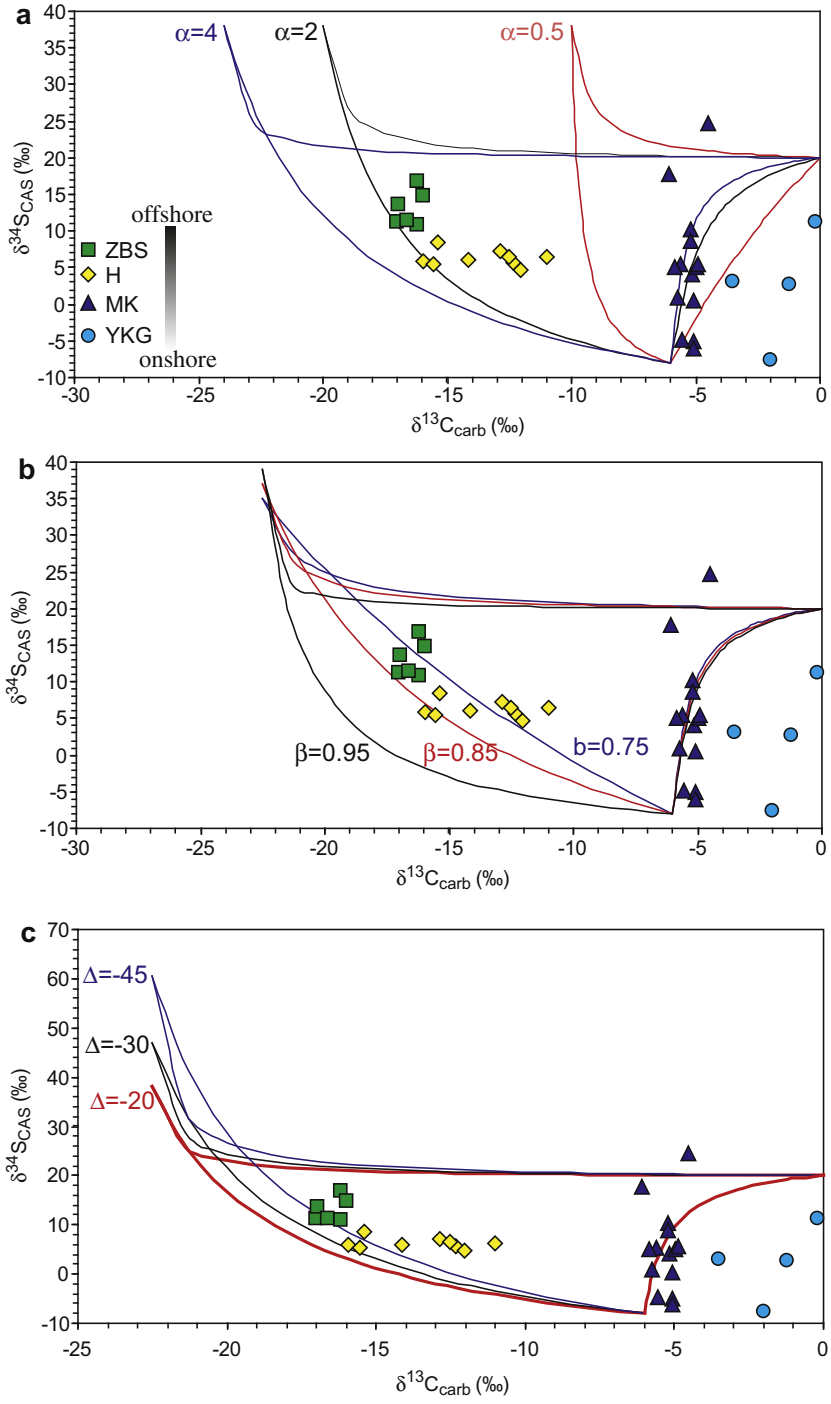

Fig. 6. Sensitivity tests. (a) The response of permissible mixing field to three different choices of $\alpha = m_{DOC}/m^{C}_{surf}$ values, with other parameters fixed at $\Delta = -20‰$ and $\beta = 0.9$. The result shows α should be $\geqslant 2$ to accommodate most of the measured data. In other words, if $m^{C}_{surf} = 2$ mM (as in modern ocean), DOC remineralization in deep-basin water (m_{DOC}) should generate additional 4 mM DIC. (b) The response of permissible mixing field to three different choices of $\beta = 0.5 \times m_{DOC}/m^{S}_{surf}$ values, with other parameters fixed at $\alpha = 3$ and $\Delta = -20‰$. The result shows that β should be $\geqslant 0.85$ to accommodate the data, suggesting that more than 85% of deep water sulfate was consumed by bacterial sulfate reduction during DOC remineralization. (c) The response of permissible mixing field to three different choices of $\Delta = \delta^{34}S_{pyrite} - \delta^{34}S_{residual\ sulfate}$ values, with other parameters fixed at $\alpha = 3$ and $\beta = 0.9$. The simulation result is not sensitive to Δ between $-20‰$ and $-40‰$. In all three tests, we kept $\delta^{13}C_{surf} = 0‰$, $\delta^{13}C_{terr} = -6‰$, $\delta^{34}S_{surf} = +20‰$, $\delta^{34}S_{terr} = -8‰$, $m^{C}_{terr}/m^{S}_{terr} = 5$, $m^{C}_{surf} = 2$ mM; and $\delta^{13}C_{DOC} = -30‰$.

fractionations ($\Delta^{34}S = \delta^{34}S_{CAS} - \delta^{34}S_{py} < 0$). Similarly, negative $\Delta^{34}S$ values have also been reported from paired sulfur isotope analyses of the cap carbonate overlying the Cryogenian Tereeken diamictite in the Quruqtagh area of

northwestern China (Shen et al., 2008) and the Ediacaran Nama group in southern Namibia (Ries et al., 2009). Shen et al. (2008) interpret that the negative $\Delta^{34}S$ in the Zhamoketi cap dolostone as reflecting deposition in a stratified basin, where CAS and pyrites were derived from different sulfur pools above and below the chemocline. In such a stratified basin, sulfate in deep-basin water is envisioned to be ^{34}S-enriched (but with a lower concentration than surface water) because of preferential removal of ^{32}S by bacterial sulfate reduction and pyrite precipitation. On the other hand, surface water had higher concentrations insofar as it was continuously replenished with ^{34}S-depleted sulfate from terrestrial weathering inputs. In this model, the ^{34}S-enriched pyrites in samples with negative $\Delta^{34}S$ values may have exclusively or predominately derived from deep water sulfate. This view, however, may not be applicable to the inverse sulfur isotope fractionation observed in samples from the Nama Group since these carbonates were deposited on shallow, well mixed shelves. Alternatively, Ries et al. (2009) interpret the Nama data (predominantly from limestone samples) in terms of aerobic reoxidation of sedimentary sulfide. Laboratory experiments of sulfide oxidation by O_2 indicate that resulting sulfate is ~5‰ lower than original sulfide (Fry et al., 1988), which could explain some reduction in the magnitude of isotopic differences between CAS and pyrite. Larger fractionations (up to 18‰ reported by Ries et al. (2009)) might result from microbial sulfide oxidation (Kaplan and Rittenberg, 1964) or a Rayleigh type pathway if the system were isolated (unlikely in this storm-dominated environment).

Nonetheless, it remains possible that both stratification-mixing (Shen et al., 2008) and aerobic reoxidation (Ries et al., 2009) may have contributed to the very low to negative $\Delta^{34}S$ values observed in the Quruqtagh sections. In the offshore sections (ZBS and H), pyrite formation was dominated by precipitation from deep-basin water with very high $\delta^{34}S_{pyrite}$ values, whereas $\delta^{34}S_{CAS}$ values reflects carbonate precipitated from shallow waters and thus are more strongly influenced by ^{34}S-depleted sulfate derived from terrestrial input, resulting in negative $\Delta^{34}S$ values. However, in the more onshore sections (YKG and MK), aerobic oxidation of sulfide (Ries et al., 2009) could have played a more important role in contributing to the observed negative $\Delta^{34}S$ values.

7. OXIDATION OF EDIACARAN OCEANS AND ISOTOPIC GRADIENT

The mixing model proposed here critically depends on two geochemical gradients: terrestrial weathering input diminishing from onshore to offshore whereas deep-basin water contribution diminishing in the opposite direction. The two geochemical gradients in turn depend on the oxidative weathering of pyrite in the terrestrial weathering input and the remineralization of DOC in the deep-basin water. Thus, the generation of both geochemical gradients has to do with the oxygenation of the Ediacaran atmosphere and the oxidation of Ediacaran oceans.

Deep-basin ^{12}C-enriched DIC derived from anaerobic oxidation of DOC played an important role in generating the carbon isotope gradient. Our simulation implies that the remineralization of deep water DOC could triple the DIC concentration (i.e. $\alpha = 2$, remineralized DOC = 4 mM, and pre-remineralization DIC = 2 mM; Fig. 6a). The remineralization would also consume >85% of deep-water sulfate (Fig. 6b). Upwelling of the ^{12}C-enriched DIC from the deep-basin water then contributed to the negative $\delta^{13}C_{carb}$ signatures preserved in Ediacaran carbonates.

Extremely negative carbonate carbon isotopes ($\delta^{13}C_{carb} \leqslant -10‰$) have been reported from many Ediacaran successions, and are interpreted as the indirect evidence for the oxidation of Ediacaran deep oceans, leading to partial remineralization of a large DOC reservoir stored in the deep ocean (Rothman et al., 2003). The best known example of such negative $\delta^{13}C_{carb}$ excursions is represented by the Shuram event, a $-10‰$ $\delta^{13}C_{carb}$ excursion from the Shuram Formation in Oman (Fike et al., 2006). Negative $\delta^{13}C_{carb}$ excursions of comparable magnitude have been reported from the middle and uppermost Doushantuo Formation in South China (Zhou and Xiao, 2007; McFadden et al., 2008), Wonoka Formation in South Australia (Calver, 2000), Krol B-C boundary in northern India (Kaufman et al., 2006), and the Rainstorm Member and middle Stirling Quartzite in Death Valley (Kaufman et al., 2007). Available geochronological constraints are inadequate to prove the synchroneity of negative excursions. Current debates center around whether *any* of these negative $\delta^{13}C_{carb}$ excursions were synchronous, how long these excursions lasted (Condon et al., 2005; Le Guerroue et al., 2005; Fike et al., 2006), and whether there were enough oxidants to account for a long-lasting (~50 million years) and global oxidation of DOC (Bristow and Kennedy, 2009).

As stated above, oxidation of Ediacaran deep oceans might also result in an onshore–offshore $\delta^{13}C$ gradient, if ^{12}C-enriched deep water is brought to shallow shelves by upwelling. Indeed, evidence for onshore–offshore $\delta^{13}C$ gradients in Neoproterozoic basins have been reported in several studies (Li et al., 1999; Jiang et al., 2007; Giddings and Wallace, 2009a,b), and such gradients are normally interpreted in term of chemical stratification, remineralization, and subsequent upwelling.

Our mixing model also places some quantitative constraints on Ediacaran ocean geochemistry. Based on our model, if the DIC concentration in the surface water was 2 mM (as in modern oceans), to generate the observed extremely negative $\delta^{13}C_{carb}$ values requires an α values of >2 (i.e., remineralization of >4 mM DOC in deep-basin water). This means that seawater sulfate concentration should be greater than 2 mM, a value that is broadly consistent with other independent estimates of seawater sulfate concentrations in Mesoproterozoic oceans (e.g., Kah et al., 2004). This moderate sulfate concentration, together with a large DOC reservoir, may have played an important role in the dynamics of the DIC system during the Neoproterozoic Era and particularly the Ediacaran Period. If the DOC was too low (e.g., 47 μM in modern oceans), the isotopic effect of DOC remineralization would be effectively buffered by a large DIC pool (e.g., 2 mM in modern oceans). In contrast, if ocean sulfate concentration was too low, then DOC remineralization would be limited by sulfate avail-

ability even if DOC was abundant in the ocean. The Ediacaran Period thus may represent a transitional interval between a largely anoxic deep ocean in the early Proterozoic to an extensively ventilated deep ocean in the Phanerozoic. It is the unique combination of a large DOC reservoir (perhaps inherited from early Proterozoic; Rothman et al., 2003) and an increasing ocean sulfate concentration (related to global oxygenation; (Halverson and Hurtgen, 2007)) that led to the highly dynamic DIC system in the Ediacaran Period.

Finally, the very existence of an onshore–offshore gradient indicates that negative $\delta^{13}C_{carb}$ excursions (with possible exception of the Shuram event) in the Ediacaran Period may be short-term local or regional events. Considering all data available, it is possible that the redox conditions of Ediacaran oceans were metastable, and several episodic oxidation events of different magnitude and duration and affecting different geographic areas may have occurred throughout the Ediacaran Period. These oxidation events may have related to oceanic upwelling, thus oxidizing only part of the deep-ocean DOC reservoir and driving surface ocean DIC (rather than whole ocean DIC) to more negative $\delta^{13}C$ values. The deep ocean might have remained anoxic until the terminal Ediacaran Period or even early Cambrian (Canfield et al., 2008; McFadden et al., 2008). This more complex scenario with multiple episodes and greater geographic variation would alleviate the problem of insufficient oxidants to drive a single long-lasting globally synchronous oxidation of the entire ocean (Bristow and Kennedy, 2009).

8. CONCLUSIONS

Coupled carbon and sulfur isotope data from the Ediacaran Hankalchough cap dolostone in the Quruqtagh area of northwestern China indicate a strong onshore–offshore gradient of $\delta^{13}C_{carb}$ and $\delta^{34}S_{CAS}$. $\delta^{13}C_{carb}$ shows a decreasing trend from onshore to offshore sections, whereas $\delta^{34}S_{CAS}$ becomes more negative and more scattered from offshore to onshore sections. The observed isotopic gradients are best interpreted in terms of a mixing model that involves three C/S sources from the upwelling of deep-basin water, surface water, and oxidative terrestrial weathering. The model simulation indicates that the carbon isotope gradient is controlled by the upwelling of ^{13}C-depleted alkalinity derived from anaerobic oxidation of DOC in deep basin, and the sulfur isotope gradient is strongly affected by the terrestrial input of ^{34}S-depleted sulfate mainly originated from oxidation of pyrite. The new data support a stratified basin with a steep geochemical gradient (Jiang et al., 2007; Giddings and Wallace, 2009a), the possibility of a large DOC reservoir in the deep ocean (Rothman et al., 2003), and enhanced oxidative terrestrial weathering. Combined with other available data, the Hankalchough data suggest that the oxidation of Ediacaran oceans was a complex process, involving multiple episodes of different magnitude and duration. Some of these oxidation events may not be globally synchronous and they each oxidized only part of the deep ocean DOC reservoir.

ACKNOWLEDGEMENTS

This work was supported by grants from National Science Foundation, NASA Exobiology Program, National Natural Science Foundation of China, Chinese Academy of Sciences, and Chinese Ministry of Science and Technology. We thank Y. Qian, J. Wang, and L. Zhang for field assistance; G. Dickens, G. Jiang, J. Sewall, Tim Lyons, and two anonymous reviewers for constructive comments; N. Han, A.M. Tilley, J. Liu, B. Williams, and C. Hebert for laboratory assistance.

REFERENCES

Balci N., Shanks, III, W. C., Mayer B. and Mandernack K. W. (2007) Oxygen and sulfur isotope systematics of sulfate produced by bacterial and abiotic oxidation of pyrite. *Geochim. Cosmochim. Acta* **71**, 3796–3811.

Bowring S., Myrow P., Landing E., Ramezani J. and Grotzinger J. (2003) Geochronological constraints on terminal Neoproterozoic events and the rise of metazoans. *Geophys. Res Abst.* **5**, 13219.

Bristow T. F. and Kennedy M. J. (2009) Carbon isotope excursions and the oxidant budget of the Ediacaran atmosphere and ocean. *Geology* **36**, 863–866.

Burdett J., Arthur M. and Richardson M. (1989) A Neogene seawater sulfur isotope age curve from calcareous pelagic microfossils. *Earth Planet. Sci. Lett.* **94**, 189–198.

Calver C. R. (2000) Isotope stratigraphy of the Ediacarian (Neoproterozoic III) of the Adelaide Rift complex, Australia, and the overprint of water column stratification. *Precambrian Res.* **100**, 121–150.

Canfield D. E. (1998) A new model for Proterozoic ocean chemistry. *Nature* **396**, 450–453.

Canfield D. E. and Raiswell R. (1991) Pyrite formation and fossil preservation.. In *Taphonomy; releasing the data locked in the fossil record* (eds. P. A. Allison and D. E. G. Briggs). Plenum Press, New York, NY, United States, pp. 337–387.

Canfield D. E., Raiswell R., Westrich J. T., Reaves C. M. and Berner R. A. (1986) The use of chromium reduction in the analysis of reduced inorganic sulfur in sediments and shales. *Chem. Geol.* **54**, 149–155.

Canfield D. E., Poulton S. W. and Narbonne G. M. (2007) Late-Neoproterozoic deep-ocean oxygenation and the rise of animal life. *Science* **315**, 92–95.

Canfield D. E., Poulton S. W., Knoll A. H., Narbonne G. M., Ross G., Goldberg T. and Strauss H. (2008) Ferruginous conditions dominated later Neoproterozoic deep-water chemistry. *Science* **321**, 949–952.

Chiba H. and Sakai H. (1985) Oxygen isotope exchange rate between dissolved sulfate and water at hydrothermal temperatures. *Geochim. Cosmochim. Acta* **49**, 993–1000.

Condon D., Zhu M., Bowring S., Wang W., Yang A. and Jin Y. (2005) U-Pb ages from the Neoproterozoic Doushantuo Formation, China. *Science* **308**, 95–98.

Corkeron M. (2007) 'Cap carbonates' and Neoproterozoic glacigenic successions from the Kimberley region, north-west Australia. *Sedimentology* **54**, 871–903.

Derry L. A. (2010) A burial diagenesis origin for the Ediacaran Shuram-Wonoka carbon isotope anomaly. *Earth Planet. Sci. Lett.* **294**, 152–162.

Dieser M., Foreman C. M., McKnight D. M., Miller P. L. and Chin Y. (2006) Microbial metabolic activity and bioavailability of dissolved organic matter under the Impact of Intense UV radiation in Pony Lake, Antarctica. *Eos Trans. AGU* **87**, B13C–1110.

Dong L., Xiao S., Shen B., Zhou C., Li G. and Yao J. (2009) Basal Cambrian microfossils from the Yangtze Gorges area (South China) and the Aksu area (Tarim Block, northwestern China). *J. Paleontol.* **83**, 30–44.

Eglinton T. I., Repeta D. J., Heinrich D. H. and Karl K. T. (2003) Organic matter in the contemporary ocean. In *The oceans and marine geochemistry* (eds. H. D. Holland and K. K. Turekian). Pergamon, Oxford, pp. 145–180.

Fike D. A. and Grotzinger J. P. (2010) A $\delta^{34}S_{SO4}$ approach to reconstructing biogenic pyrite burial in carbonate-evaporite basins: an example from the Ara Group, Sultanate of Oman. *Geology* **38**, 371–374.

Fike D. A., Grotzinger J. P., Pratt L. M. and Summons R. E. (2006) Oxidation of the Ediacaran Ocean. *Nature* **444**, 744–747.

Fry B., Ruf W., Gest H. and Hayes J. M. (1988) Sulfur isotope effects associated with oxidation of sulfide by O_2 in aqueous solution. *Chem. Geol. Isot. Geosci. Sect.* **73**, 205–210.

Gao Z. and Zhu S. (1984) *Precambrian geology in Xinjiang, China*. Xinjiang People's Publishing House, Urumuqi, China.

Giddings J. A. and Wallace M. W. (2009a) Facies-dependent $\delta^{13}C$ variation from a Cryogenian platform margin, South Australia: evidence for stratified Neoproterozoic oceans? *Palaeogeogr. Palaeoclimatol. Palaeoecol.* **271**, 196–214.

Giddings J. A. and Wallace M. W. (2009b) Sedimentology and C-isotope geochemistry of the 'Sturtian' cap carbonate, South Australia. *Sediment. Geol.* **216**, 1–14.

Goldberg T., Poulton S. W. and Strauss H. (2005) Sulphur and oxygen isotope signatures of late Neoproterozoic to early Cambrian sulphate, Yangtze Platform, China: diagenetic constraints and seawater evolution. *Precambrian Res.* **137**, 223–241.

Halverson G. P. and Hurtgen M. T. (2007) Ediacaran growth of the marine sulfate reservoir. *Earth Planet. Sci. Lett.* **263**, 32–44.

Halverson G. P., Hoffman P. F., Schrag D. P., Maloof A. C. and Rice A. H. N. (2005) Toward a Neoproterozoic composite carbon-isotope record. *Geol. Soc. Am. Bull.* **117**, 1181–1207.

Halverson G. P., Dudás F. Ö., Maloof A. C. and Bowring S. A. (2007) Evolution of the 87Sr/86Sr composition of Neoproterozoic seawater. *Palaeogeogr. Palaeoclimatol. Palaeoecol.* **256**, 103–129.

Hoffman P. F. and Li Z.-X. (2009) A palaeogeographic context for Neoproterozoic glaciation. *Palaeogeogr. Palaeoclimatol. Palaeoecol.* **277**, 158–172.

Hoffman P. F., Kaufman A. J., Halverson G. P. and Schrag D. P. (1998) A Neoproterozoic snowball Earth. *Science* **281**, 1342–1346.

Hoffman P. F., Halverson G. P., Domack E. W., Husson J. M., Higgins J. A. and Schrag D. P. (2007) Are basal Ediacaran (635 Ma) post-glacial "cap dolostones" diachronous? *Earth Planet. Sci. Lett.* **258**, 114–131.

Hoffmann K.-H., Condon D. J., Bowring S. A. and Crowley J. L. (2004) U-Pb zircon date from the Neoproterozoic Ghaub Formation, Namibia: Constraints on Marinoan glaciation. *Geology* **32**, 817–820.

Hyde W. T., Crowley T. J., Baum S. K. and Peltier W. R. (2000) Neoproterozoic "snowball Earth" simulations with a coupled climate/ice-sheet model. *Nature* **405**, 425–429.

Jacobsen S. B. and Kaufman A. J. (1999) The Sr, C and O isotopic evolution of Neoproterozoic seawater. *Chem. Geol.* **161**, 37–57.

Jiang G., Kennedy M. J. and Christie-Blick N. (2003) Stable isotopic evidence for methane seeps in Neoproterozoic postglacial cap carbonates. *Nature* **426**, 822–826.

Jiang G., Kaufman A. J., Christie-Blick N., Zhang S. and Wu H. (2007) Carbon isotope variability across the Ediacaran Yangtze platform in South China: implications for a large surface-to-deep ocean $\delta^{13}C$ gradient. *Earth Planet. Sci. Lett.* **261**, 303–320.

Johnston D. T., Wolfe-Simon F., Pearson A. and Knoll A. H. (2009) Anoxygenic photosynthesis modulated Proterozoic oxygen and sustained Earth's middle age. *Proc. Natl. Acad. Sci. USA* **106**, 16925–16929.

Kah L. C., Lyons T. W. and Frank T. D. (2004) Low marine sulphate and protracted oxygenation of the Proterozoic biosphere. *Nature* **431**, 834–838.

Kampschulte A. and Strauss H. (2004) The sulfur isotopic evolution of Phanerozoic seawater based on the analysis of structurally substituted sulfate in carbonates. *Chem. Geol.* **204**, 255–286.

Kampschulte A., Bruckschen P. and Strauss H. (2001) The sulphur isotopic composition of trace sulphates in Carboniferous brachiopods: implications for coeval seawater, correlation with other geochemical cycles and isotope stratigraphy. *Chem. Geol.* **205**, 149–173.

Kaplan I. R. and Rittenberg S. C. (1964) Microbiological fractionation of sulphur isotopes. *J. Gen. Microbiol.* **34**, 195–212.

Kaufman A. J. and Knoll A. H. (1995) Neoproterozoic variations in the C-isotope composition of sea water: stratigraphic and biogeochemical implications. *Precambrian Res.* **73**, 27–49.

Kaufman A. J., Knoll A. H. and Awramik S. M. (1992) Biostratigraphic and chemostratigraphic correlation of Neoproterozoic sedimentary successions: Upper Tindir Group, northwestern Canada, as a test case. *Geology* **20**, 181–185.

Kaufman A. J., Jacobsen S. B. and Knoll A. H. (1993) The Vendian record of Sr and C isotopic variations in seawater: implications for tectonics and paleoclimate. *Earth Planet. Sci. Lett.* **120**, 409–430.

Kaufman A. J., Jiang G., Christie-Blick N., Banerjee D. M. and Rai V. (2006) Stable isotope record of the terminal Neoproterozoic Krol platform in the Lesser Himalayas of northern India. *Precambrian Res.* **147**, 156–185.

Kaufman A. J., Corsetti F. A. and Varni M. A. (2007) The effect of rising atmospheric oxygen on carbon and sulfur isotope anomalies in the Neoproterozoic Johnnie Formation, Death Valley, USA. *Chem. Geol.* **237**, 47–63.

Knauth L. P. and Kennedy M. J. (2009) The late Precambrian greening of the Earth. *Nature* **460**, 728–732.

Le Guerroue E., Allen P. A., Cozzi A., Etienne J. L. and Fanning M. (2005) 50-Myr recovery from the largest negative $\delta^{13}C$ excursion in the Ediacaran ocean. *Terra Nova* **18**, 147–153.

Li H. and Dong Y. (1991) Sedimentary features of the Sinian Zhamoketi Formation in the Middle Quruqtagh area of Xinjiang. *Xinjiang Geol.* **9**, 340–351.

Li R., Chen J., Zhang S., Lei J., Shen Y. and Chen X. (1999) Spatial and temporal variations in carbon and sulfur isotopic compositions of Sinian sedimentary rocks in the Yangtze platform, South China. *Precambrian Res.* **97**, 59–75.

Li C., Love G. D., Lyons T. W., Fike D. A., Sessions A. L. and Chu X. (2010) A stratified redox model for the Ediacaran Ocean. *Science* **328**, 80–83.

Logan G. A., Hayes J. M., Hieshima G. B. and Summons R. E. (1995) Terminal Proterozoic reorganization of biogeochemical cycles. *Nature* **376**, 53–57.

Marenco P. J., Corsetti F. A., Hammond D. E., Kaufman A. J. and Bottjer D. J. (2008a) Oxidation of pyrite during extraction of carbonate associated sulfate. *Chem. Geol.* **247**, 124–132.

Marenco P. J., Corsetti F. A., Kaufman A. J. and Bottjer D. J. (2008b) Environmental and diagenetic variations in carbonate associated sulfate: an investigation of CAS in the Lower Triassic of the western USA. *Geochim. Cosmochim. Acta* **72**, 1570–1582.

Mazumdar A., Goldberg T. and Strauss H. (2008) Abiotic oxidation of pyrite by Fe(III) in acidic media and its implica-

tions for sulfur isotope measurements of lattice-bound sulfate in sediments. *Chem. Geol.* **253**, 30–37.

McFadden K. A., Huang J., Chu X., Jiang G., Kaufman A. J., Zhou C., Yuan X. and Xiao S. (2008) Pulsed oxidation and biological evolution in the Ediacaran Doushantuo formation. *Proc. Natl. Acad. Sci. USA* **105**, 3197–3202.

Meybeck M., Heinrich D. H. and Karl K. T. (2003) Global occurrence of major elements in rivers. vol. 5. In *Surface and ground water, weathering, and soils* (eds. H. D. Holland and K. K. Turekian). Pergamon, Oxford, pp. 207–223.

Narbonne G. M. and Gehling J. G. (2003) Life after snowball: the oldest complex Ediacaran fossils. *Geology* **31**, 27–30.

Peltier W. R., Liu Y. and Crowley J. W. (2007) Snowball Earth prevention by dissolved organic carbon remineralization. *Nature* **450**, 813–819.

Pingitore, Jr., N. E., Meitzner G. and Love K. M. (1995) Identification of sulfate in natural carbonates by X-ray absorption spectroscopy. *Geochim. Cosmochim. Acta* **59**, 2477–2483.

Ries J. B., Fike D. A., Pratt L. M., Lyons T. W. and Grotzinger J. P. (2009) Superheavy pyrite ($\delta^{34}S_{pyr}>\delta^{34}S_{CAS}$) in the terminal Proterozoic Nama Group, southern Namibia: a consequence of low seawater sulfate at the dawn of animal life. *Geology* **37**, 743–746.

Rothman D. H., Hayes J. M. and Summons R. E. (2003) Dynamics of the Neoproterozoic carbon cycle. *Proc. Natl. Acad. Sci. USA* **100**, 8124–8129.

Schrag D. P., Berner R. A., Hoffman P. F. and Halverson G. P. (2002) On the initiation of a snowball Earth. *Geochem. Geophys. Geosyst.* **3**. doi:10.1029/2001GC000219.

Scott C., Lyons T. W., Bekker A., Shen Y., Poulton S. W., Chu X. and Anbar A. D. (2008) Tracing the stepwise oxygenation of the Proterozoic ocean. *Nature* **452**, 456–459.

Shen B., Xiao S., Dong L., Zhou C. and Liu J. (2007) Problematic macrofossils from Ediacaran successions in the North China and Chaidam blocks: implications for there evolutionary root and biostratigraphic significance. *J. Paleontol.* **81**, 1396–1411.

Shen B., Xiao S., Bao H., Kaufman A. J., Zhou C. and Wang H. (2008) Stratification and mixing of the post-glacial Neoproterozoic Ocean: evidence from carbon and sulfur isotopes in a cap dolostone from northwest China. *Earth Planet. Sci. Lett.* **265**, 209–228.

Shen B., Xiao S., Zhou C., Kaufman A. J. and Yuan X. (2010) Carbon and sulfur isotope chemostratigraphy of the Neoproterozoic Quanji Group of the Chaidam Basin, NW China: basin stratification in the aftermath of an Ediacaran glaciation postdating the Shuram event? *Precambrian Res.* **177**, 241–252.

Swanson-Hysell N. L., Rose C. V., Calmet C. C., Halverson G. P., Hurtgen M. T. and Maloof A. C. (2010) Cryogenian glaciation and the onset of carbon-isotope decoupling. *Science* **328**, 608–611.

Van Stempvoort D. R. and Krouse H. R. (1994) Controls of sulfate $\delta^{18}O$: a general model and application to specific environments. In *Environmental geochemistry of sulfide oxidation* (eds. C. N. Alpers and D. W. Blowes). American Chemical Society, Washington, DC, pp. 446–480.

Wang Y., Zhuang Q., Shi C., Liu J. and Zheng L. (1980) Quanji Group along the northern border of Chaidamu Basin. In *Research on Precambrian Geology Sinian Suberathem in China*. Tianjin Institute of Geology and Mineral Resources, Tianjin, pp. 214–230.

Wang J., Jiang G., Xiao S., Li Q. and Wei Q. (2008) Carbon isotope evidence for widespread methane seeps in the ca. 635 Ma Doushantuo cap carbonate in south China. *Geology* **36**, 347–350.

Xiao S. (2008) Geobiological events in the ediacaran period. In *From evolution to geobiology: research questions driving paleontology at the start of a new century* (eds. P. H. Kelly and R. K. Bambach). The Paleontological Society, New Haven, pp. 85–104.

Xiao S., Bao H., Wang H., Kaufman A. J., Zhou C., Li G., Yuan X. and Ling H. (2004) The Neoproterozoic Quruqtagh Group in eastern Chinese Tianshan: evidence for a post-Marinoan glaciation. *Precambrian Res.* **130**, 1–26.

Xu B., Jian P., Zheng H., Zou H., Zhang L. and Liu D. (2005) U-Pb zircon geochronology and geochemistry of Neoproterozoic volcanic rocks in the Tarim Block of northwest China: implications for the breakup of Rodinia supercontinent and Neoproterozoic glaciations. *Precambrian Res.* **136**, 107–123.

Xu B., Xiao S., Zou H., Chen Y., Li Z.-X., Song B., Liu D., Zhou C. and Yuan X. (2009). *SHRIMP zircon U-Pb age constraints on Neoproterozoic Quruqtagh diamictites in NW China Precambrian Res.* **168**, 247–258.

Yao J., Xiao S., Yin L., Li G. and Yuan X. (2005) Basal Cambrian microfossils from the Yurtus and Xishanblaq formations (Tarim, north-west China): systematic revision and biostratigraphic correlation of *Micrhystridium*-like acritarchs from China. *Palaeontology* **48**, 687–708.

Zhou C. and Xiao S. (2007) Ediacaran $\delta^{13}C$ chemostratigraphy of South China. *Chem. Geol.* **237**, 89–108.

Associate editor: Timothy W. Lyons